Available online at www.sciencedirect.com
SCIENCE DIRECT®
ELSEVIER
International Journal of Multiphase Flow 31 (2005) 1304–1328
International Journal of Multiphase Flow
www.elsevier.com/locate/ijmulflow

Development of co-current air–water flow in a vertical pipe

D. Lucas *, E. Krepper, H.-M. Prasser

Forschungszentrum Rossendorf e.V., Institute of Safety Research, P.O. Box 510 119, D-01314 Dresden, Germany

Received 25 January 2005; received in revised form 11 July 2005

Abstract

Measurements of the cross-sectional distribution of the gas fraction and bubble size distributions were conducted in a vertical pipe with an inner diameter of 51.2 mm and a length of about 3 m for air/water bubbly and slug flow regimes. The use of a wire-mesh sensor obtained a high resolution of the gas fraction data in space as well as in time. From this data, time averaged values for the two-dimensional gas fraction profiles were decomposed into a large number of bubble size classes. This allowed the extraction of the radial gas fraction profiles for a given range of bubble sizes as well as data for local bubble size distributions. The structure of the flow can be characterized by such data. The measurements were performed for up to 10 different inlet lengths and for about 100 combinations of gas and liquid volume flow rates. The data is very useful for the development and validation of meso-scale models to account for the forces acting on a bubble in a shear liquid flow and models for bubble coalescence and break-up. Such models are necessary for the validation of CFD codes for the simulation of bubbly flows.

Keywords: Bubble flow; Vertical pipe flow; Experimental database; Bubble size distribution

1. Introduction

The increasing performance and memory capacity of modern computer progressively expands the possibilities of applying CFD codes to two-phase flow problems. However there are still

* Corresponding author. Tel.: +49 351 260 2047; fax: +49 351 260 2383.
E-mail address: d.lucas@fz-rossendorf.de (D. Lucas).

0301-9322/$ - see front matter
doi:10.1016/j.ijmultiphaseflow.2005.07.004

deficiencies in appropriate models for describing the complex phenomena of interaction between the phases. In case of bubbly flow and especially with higher void fractions with slug flow, the codes must be equipped with constitutive laws that describe the interaction between the gaseous and the liquid phases in a detailed way (Lucas et al., 2001a,b, 2003a,b). The widespread assumption of mono-dispersed bubble flow yields satisfactory agreement to experiments only for low gas fractions. Experimental (Tomiyama, 1998) and theoretical (Ervin and Tryggvason, 1997) investigations for vertical pipes have shown that the probability of radial residence of a bubble strongly depends on their diameter. For a vertical upward flow smaller bubbles tend to move towards the wall, while large bubbles are preferably found in the centre of the tube. This was observed for single bubbles by Tomiyama (1998). In our experiments, the investigation of bubble sizes and their preferred radial residence confirmed this observation in a multi-disperse flow (Prasser et al., 2000, 2002). For the air–water system at ambient conditions a change from wall peak to core peak of the radial gas fraction profile was found to occur at a bubble diameter of about 5–6 mm (Tomiyama, 1998). This resulted in a relationship between bubble size distributions and the location within the pipe cross-section and in turn the radial gas fraction profiles, which depend on the bubble size. As shown by Lucas et al. (2003b) this is a key phenomena for the appropriate simulation of the transition from bubble to slug flow in case of vertical pipes. The development of the flow pattern along the flow path mainly depends on the forces acting on the bubbles and on bubble coalescence and bubble break-up.

For the development and validation of appropriate models for the forces acting on a bubble and for local bubble coalescence and fragmentation, data for different local flow field situations are needed. In the case of vertical co-current pipe flow the radial flow field is symmetrically stable over a quite long distance. Therefore, this type of flow is well suited for the investigation. Accordingly there are a large number of publications regarding measurements on two-phase flow within vertical pipes of different diameters (e.g. Sekoguchi and Mori, 1997; Chang et al., 1998; Hibiki and Ishii, 1999; Ohnuki and Akimoto, 2000; Yoneda et al., 2000). The new quality of the measurements discussed in the present paper, results from the high resolution of the data space and time. The high resolution was obtained using fast wire-mesh sensors developed by the Forschungszentrum Rossendorf e.V. (Prasser et al., 1998, 2001). This measuring technique allows the resolution of single bubbles simultaneously in the entire cross-section of the pipe. The knowledge on the location as well as the size of single bubbles is used to evaluate time averaged distributions in their dependence on the location as well as their size.

To investigate the development of the flow along the pipe in dependency on the liquid flow field and the gas volume fraction; measurements were made for 99 combinations of the gas and liquid volume flow rates. Up to 10 different distances between the gas injection device and the wire mesh sensor were considered.

The data has been used to test and validate meso-scale models for the forces acting on bubbles in the liquid shear field (Lucas et al., 2004; Lucas and Prasser, 2004). Different models were tested by a simplified model to investigate their dependency on the volumetric flow rates over a wide range of values. Selected combinations of volume flow rates were defined as test cases for the validation of the implementation of models for bubble forces in CFX-5 in the framework of cooperation with the developer (Shi et al., 2004; Frank et al., 2004). As discussed by Lucas et al. (2003b) for an appropriate modelling of the development of the flow, a number of bubble classes have to be considered. An extension of the homogeneous MUSIG model, which was implemented

in CFX-4, was proposed for the further development of CFX-5 (Krepper et al., 2005). In future the data will be also used to test and validate models for bubble coalescence and break up.

2. Experimental setup and instrumentation

The evolution of the two-phase flow was studied in a vertical tube with an inner diameter of 51.2 mm that was supplied with air–water mixture at 30 °C. The test section is part of a test loop shown in Fig. 1. The main components of the facility are a circulation pump with a maximum capacity of approximately 30 m^3/h, the vertical test section, a horizontal test section and a cyclone-separator. The facility can be operated either with air–water mixture at a constant temperature or with steam–water mixture at a pressure of up to 2.5 MPa and a maximum temperature of 225 °C. The vertical test section has a maximum length of about 4 m. Since the air injection is located above a heater section, the maximum inlet length during the tests is limited to about 3.5 m.

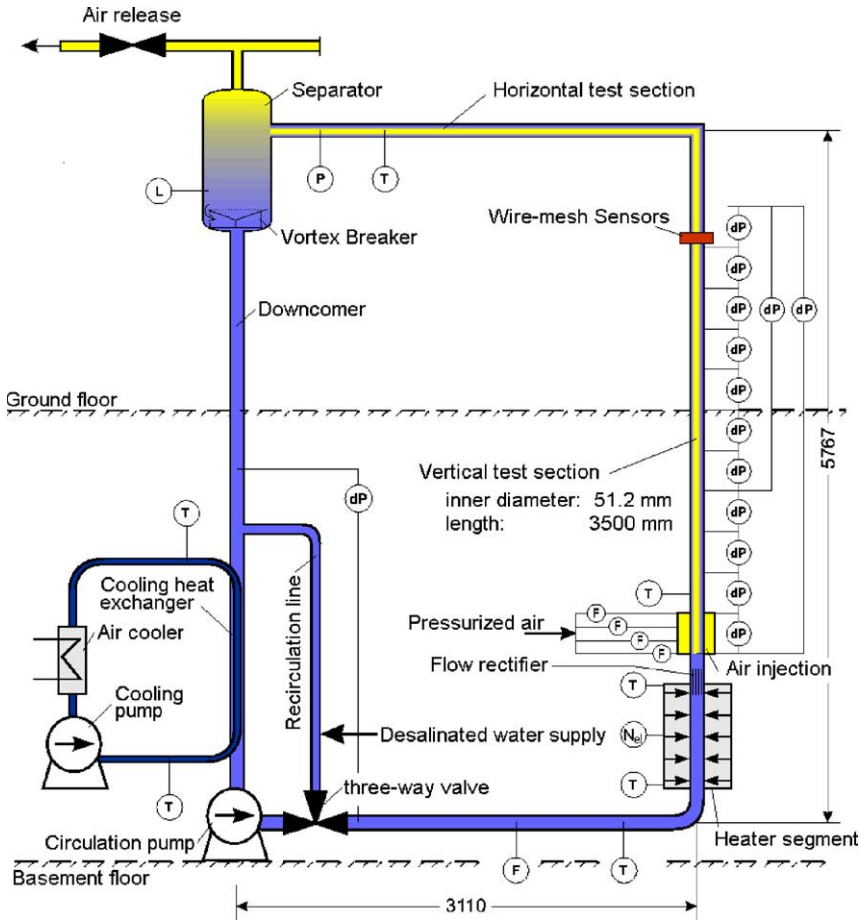

Fig. 1. Scheme of the MTLoop facility.

Upstream of the air injection is a flow rectifier. The volume flow rates are controlled by an ultrasonic flow meter for the water and hot wire flow rate sensors for the air. To vary the air volume flow rate the air supply is fed in to the test section via four separate lines. Each of the lines is designed for a certain range of volume flow rates, thus enabling accurate control of the air flow over the entire range.

The distance between sensor and air injection was varied from 0.03 m to 3.03 m (inlet lengths 0.6–60 L/D). Stationary flow rates of air and water were used. Gas and liquid superficial velocities were varied in a wide range. About 100 combinations of the superficial velocities were considered. They include stable bubbly flow, finely dispersed bubbly flow and slug flow at the upper end of the pipe. Transitions between the flow regimes were observed within the pipe.

Data was acquired by an electrode wire-mesh sensor (Fig. 2) that measured the instantaneous conductivity distribution (Prasser et al., 1998, 2001). Two planar electrode grids with 24 parallel electrode wires each (diameter 120 μm) are placed at an axial distance of 1.5 mm behind each other with the wires of one grid in perpendicular to the wires of the other grid. During signal acquisition, each cross-point of a wire of the first grid to a wire of the second grid is asked for conductivity in a successive order. The conductivity is a measure for the gas volume fraction. The entire cross-sectional distribution of the gas volume fraction is measured at a high frequency. For this sensor assembly, 2500 cross-sectional frames per second can be recorded. The spatial resolution is given by the pitch of the electrode wires and equals 2 mm for the sensor that was used

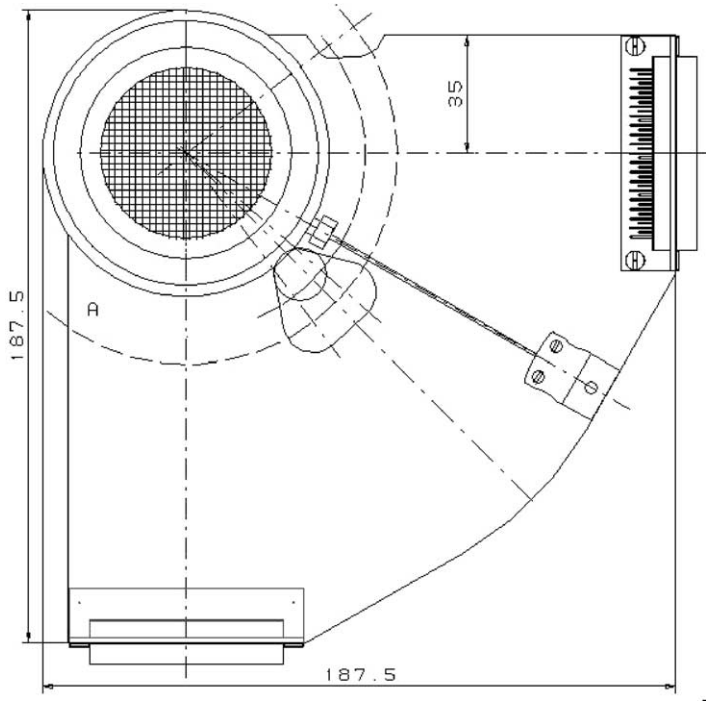

Fig. 2. Wire-mesh sensor.

here. Two identical sensors were put in a distance of 36 mm behind each other to measure gas velocities by correlating the signals obtained.

The sensor delivers a sequence of two-dimensional distributions of the local instantaneous conductivity, measured in each mesh formed by two crossing wires i and j. Local instantaneous gas fractions are calculated assuming a linear dependence between gas fraction and conductivity. The result is a three-dimensional data array i, j, k where k is the number of the instantaneous gas fraction distribution in the time sequence. According to the number of electrode wires of 24×24, the

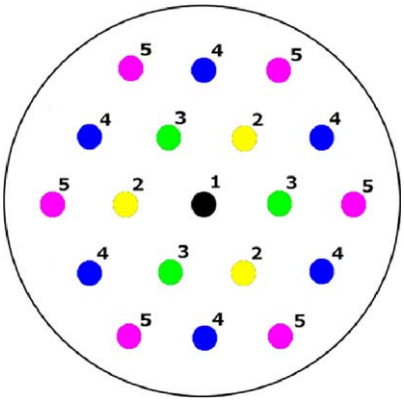

Fig. 3. Distribution of the capillaries of the gas injection device over the cross-section of the pipe. The numbers denote the groups, which can be switched of separately.

Water Superficial Velocity J / m/s	Air Superficial Velocity 0.0025	0.0040	0.0062	0.0096	0.0151	0.0235	0.0368	0.0574	0.0898	0.140	0.219	0.342	0.534
4.047	11	22	33	44	55	66	77	88	99	110	121	132	143
2.554	10	21	32	43	54	65	76	87	98	109	120	131	142
1.611	9	20	31	42	53	64	75	86	97	108	119	130	141
1.017	8	19	30	41	52	63	74	85	96	107	118	129	140
0.641	7	18	29	40	51	62	73	84	95	106	117	128	139
0.405	6	17	28	39	50	61	72	83	94	105	116	127	138
0.255	5	16	27	38	49	60	71	82	93	104	115	126	137
0.161	4	15	26	37	48	59	70	81	92	103	114	125	136
0.102	3	14	25	36	47	58	69	80	91	102	113	124	135
0.0641	2	13	24	35	46	57	68	79	90	101	112	123	134
0.0405	1	12	23	34	45	56	67	78	89	100	111	122	133
0	N01	N02	N03	N04	N05	N06	N07	N08	N09	N10	N11	N12	N13

Group of capillaries 1
Group of capillaries 2
Groups of capillaries 1 + 2
Groups of capillaries 2 + 3
Groups of capillaries 1 + 2 + 3
Groups of capillaries 1 +2 + 4
All capillaries

Fig. 4. Matrix of the combinations of superficial velocities measured and assignment of the groups of capillaries used for the gas injection.

cross-sectional frame number of 2500 per second and the measuring time of 10 s this matrix has the dimension $24 \times 24 \times 25{,}000$. Different averaging procedures enabled a further condensation of the data.

Table 1
Parameter for the different flow pattern, shown at Fig. 5

Test no.	J_L (m/s)	J_G (m/s)	Flow pattern
121	4.047	0.2190	Finely dispersed
039	0.405	0.0096	Bubbly flow with wall peak
083	0.405	0.0574	Bubbly flow in the transition region
118	1.017	0.2190	Bubbly flow with centre (core) peak
129	1.017	0.3420	Bubbly flow with a bimodal bubble size distribution
140	1.017	0.5340	Slug flow

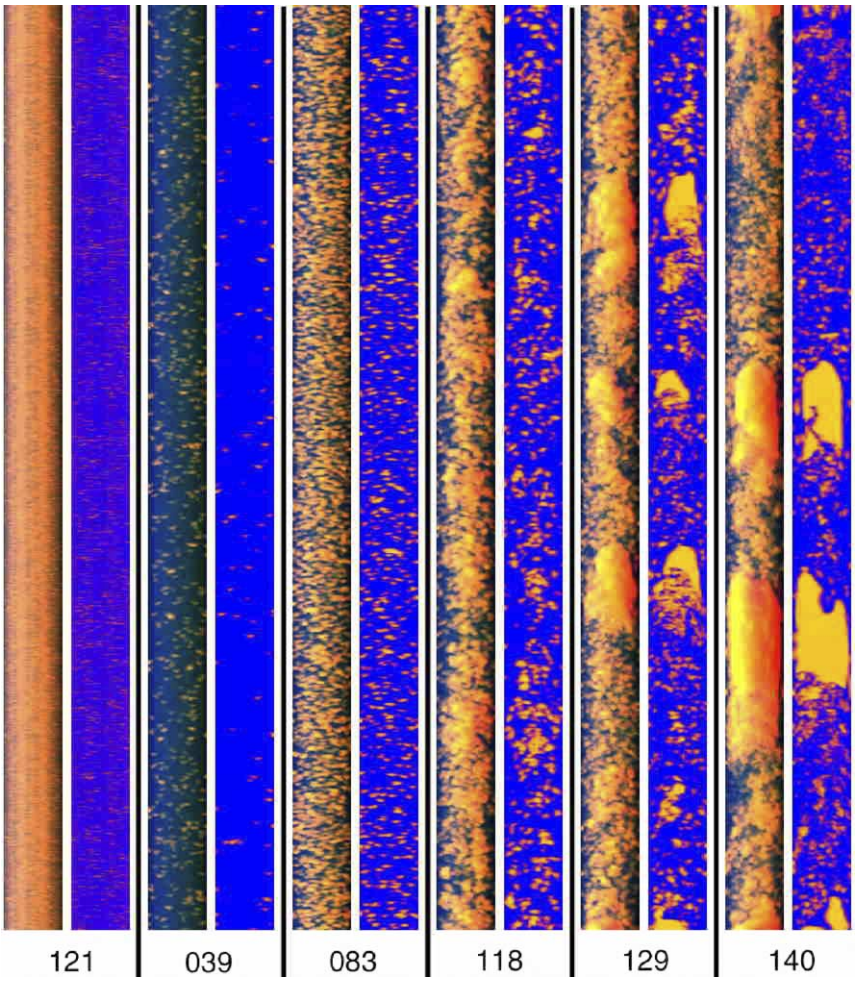

Fig. 5. Examples for the observed flow pattern (parameter see Table 1).

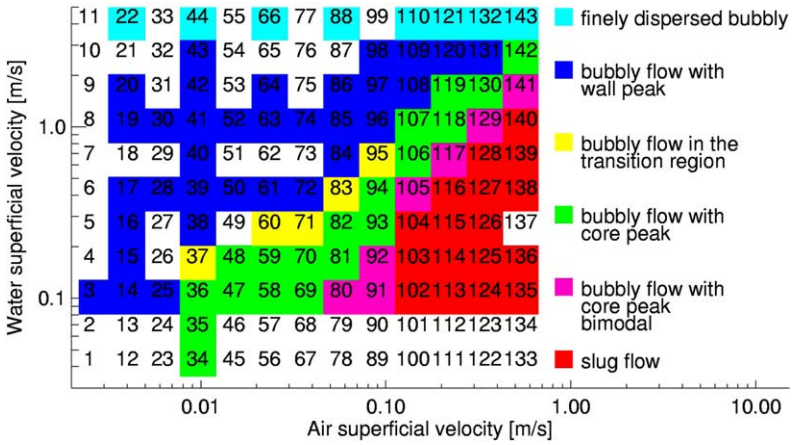

Fig. 6. Measured flow pattern map for the upper end of the pipe ($L/D = 59.2$).

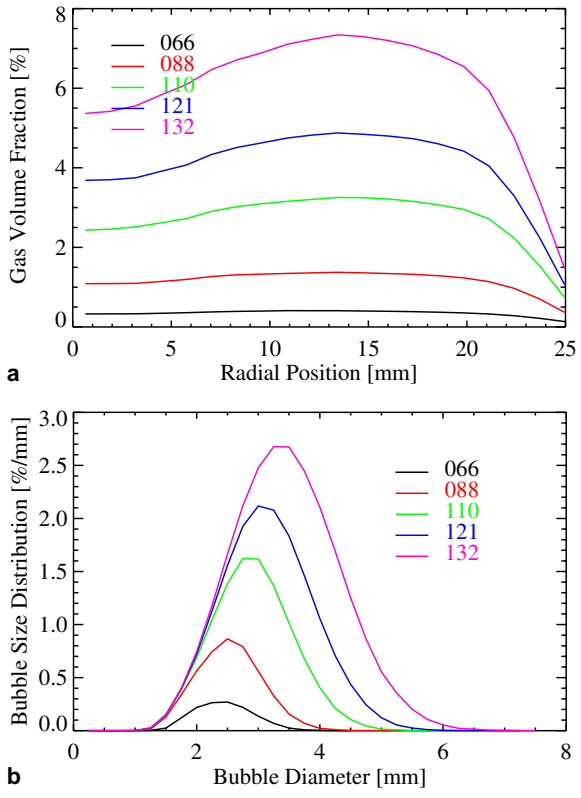

Fig. 7. Radial gas volume fraction profiles and bubble size distributions for finely dispersed flow. (Numbers for the points in the measuring matrix see Fig. 4.)

A special procedure, described by Prasser et al. (2001) allows the identification of single bubbles and the determination of their volume V_b and the equivalent bubble diameter defined by:

$$d_b = \sqrt[3]{\frac{6}{\pi} V_b}. \tag{1}$$

Using this procedure bubble size distributions as well as gas volume fraction profiles for bubbles within a predefined interval of bubble sizes can be calculated, the latter by using the method described by Prasser et al. (2002).

For the calculation of bubble size distributions, the equivalent bubble diameter is subdivided into intervals and the contribution of each individual bubble to the gas volume fraction is evaluated for each interval. This gives bubble size distributions that are related to the gas volume fraction instead of bubble size distributions related to the bubble number density. The latter has the disadvantage of poorly reflecting the number of large bubbles, since the number density of small bubbles is much higher. According to this definition of the bubble size distribution

$$h(d_b) = \frac{d\alpha}{d d_b}, \tag{2}$$

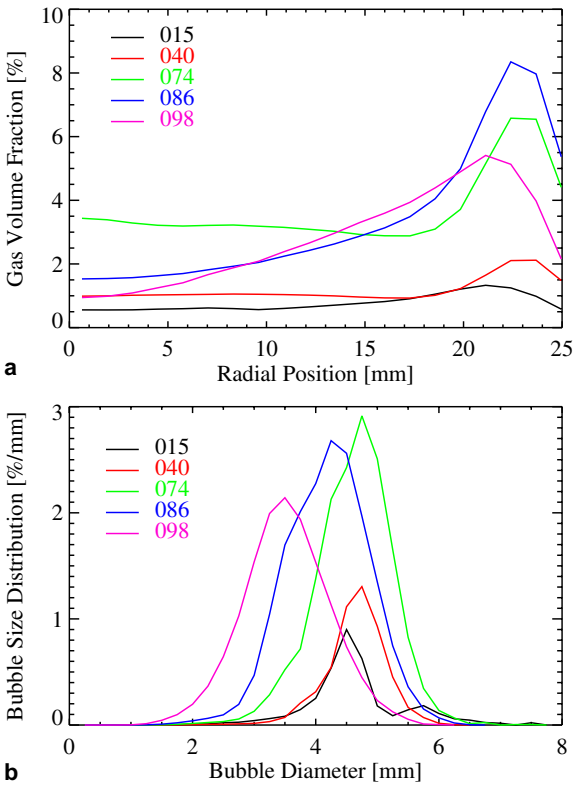

Fig. 8. Radial gas volume fraction profiles and bubble size distributions for bubbly flow with wall peak. (Numbers for the points in the measuring matrix see Fig. 4.)

the integral over the distribution yields the total gas volume fraction

$$\alpha = \int_0^\infty h(d_b)\,\mathrm{d}d_b. \tag{3}$$

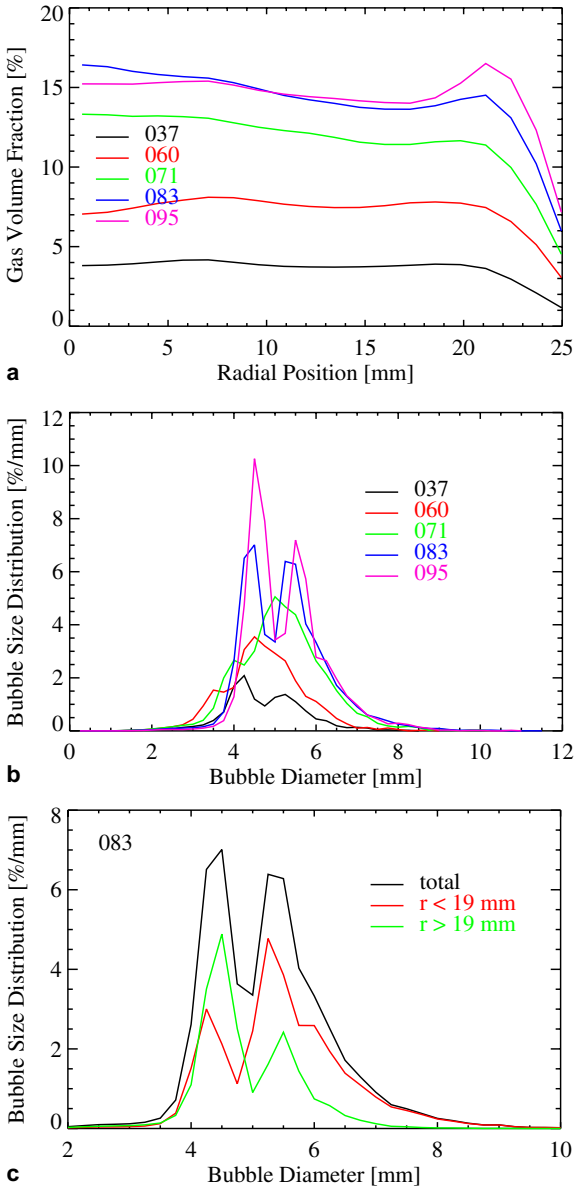

Fig. 9. Radial gas volume fraction profiles and bubble size distributions for bubbly flow in the transition region. (Numbers for the points in the measuring matrix see Fig. 4.) The last figure compares the bubble size distribution averaged over the total pipe cross-section with bubble size distributions for the inner (red curve) and the outer (green curve) region of the pipe (for interpretation of the references in colour in this figure, the reader is referred to the web version of this article).

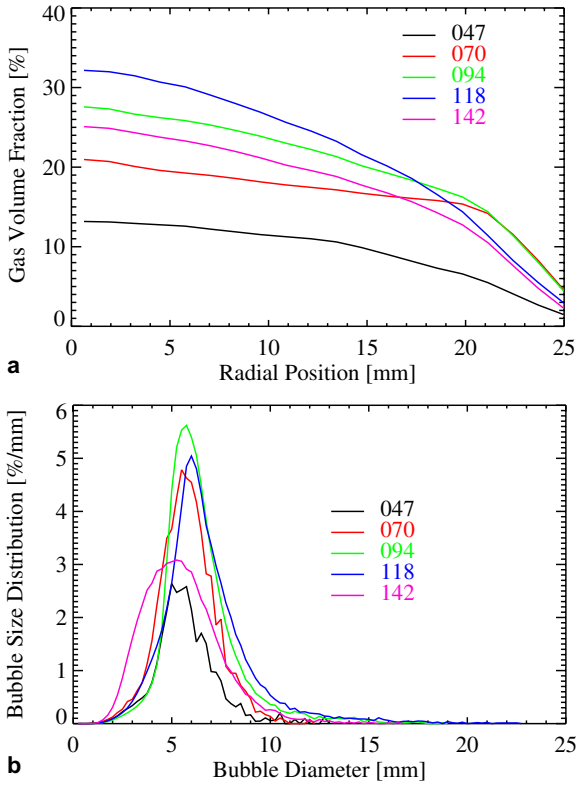

Fig. 10. Radial gas volume fraction profiles and bubble size distributions for bubbly flow with centre peak, but monomodal bubble size distribution. (Numbers for the points in the measuring matrix see Fig. 4.)

The interaction of the gas bubbles with the sensor was investigated by help of another facility specially designed for this purpose. A wire-mesh sensor was integrated into a rectangular test channel that was made of organic glass. The sensor signal was compared with high speed video pictures. As expected, the sensor cuts the bubbles, which results in the appearance of a cloud of small bubbles. Though some of the small fragments recombine, the sensor heavily disturbs the bubbles. This was clearly visible in the high-speed image sequences, while the signals of the sensor represented the bubbles still in their undisturbed shape despite of the sensor induced fragmentation. More detailed results of these investigations are reported by Prasser et al. (2001). Therefore, the measurements in the vertical pipe for different inlet lengths cannot be made simultaneously. Instead, the sensor has to be moved for each height position. For this reason first the measurements for all the combinations of superficial velocities were done for a fixed inlet length and then the sensor was repositioned to the next inlet length. This means that the development of flow pattern along the pipe was observed over several different experimental runs. Therefore, a great deal of effort was made to ensure the accurate reproducibility of the boundary conditions, to guarantee that the measurements taken at different height positions but of identical volume flow rates are comparable.

Further detailed uncertainty analyses were made by comparing the data with measurements obtained by an ultra-fast X-ray tomograph (Prasser et al., 2005a).

3. Experimental database

3.1. Pre-tests

The database discussed in this paper is a part of a database of test series. The reproducibility of the experiments was checked in extensive preliminary tests. In the first experimental runs a wire-mesh sensor with 16×16 electrode wires (pitch of the electrodes 3 mm) was used. Three different injection devices were applied: (a) small capillaries (inner diameter 0.8 mm) equally distributed over the cross-section, (b) 1 mm holes circumferential distributed over the tube and (c) 4 mm holes distributed around the circumference distributed over the tube. The bubbles generated by the injection devices (a) and (b) are of similar size, whereas the bubbles generated by injection device (c) are larger. It was shown, that the radial gas fraction profile and the bubble size distribution at the upper end of the pipe strongly depend on the initial bubble size, but are nearly independent of the radial location of the gas injection (capillaries equal distributed over the pipe cross-section of the pipe or orifices in the tube wall). All the injection devices are axis-symmetrical. Nevertheless in case of small gas volume flow rates an asymmetrical injection was observed, because not all the capillaries or orifices fed. For this reason in the main experimental run a gas injection device with

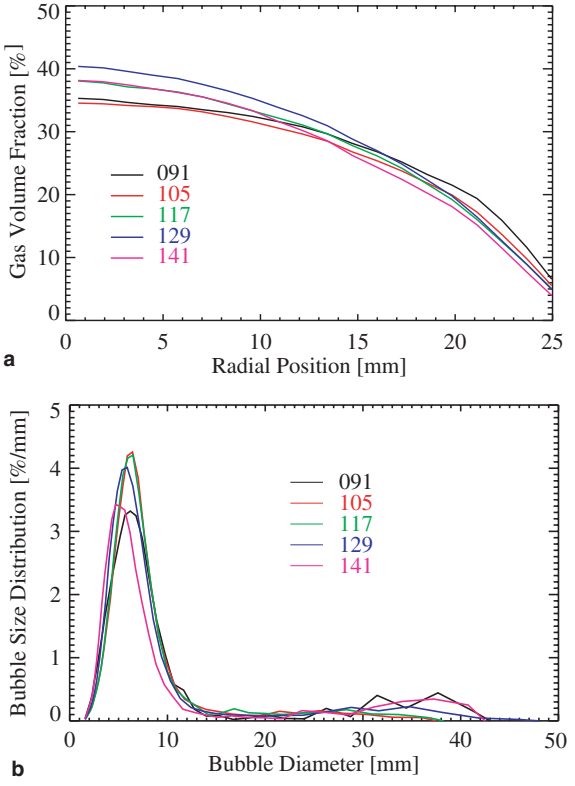

Fig. 11. Radial gas volume fraction profiles and bubble size distributions for bubbly flow with centre peak and bimodal bubble size distribution. (Numbers for the points in the measuring matrix see Fig. 4.)

19 capillaries equal distributed over the pipe cross-section of the pipe was used, but the capillaries were divided into five groups, which can switched off separately (Fig. 3). For small gas volume flow rates the number of feeding capillaries was reduced which were in any case axis-symmetric arranged. Thus a symmetrical injection was ensured for all the tests. The groups of capillaries, which were to be used, were determined by a special pre-test run, at which the sensor was close (30 mm) to the injection device. The sensor signals then showed the gas injection from the single capillaries (compare Fig. 13).

The pre-tests also indicated that the reproducibility strongly depends on the water quality. The bubble coalescence is very sensitive to small amounts of impurities. For this reason much effort was done to refresh the deionised water for each experimental run. In the result of the pre-tests a good reproducibility and also a good consistency between the data measured by the 16×16 sensor and the 24×24 sensor were achieved.

3.2. Test matrix

The development of the flow along the flow path was investigated for 89 combinations of gas and liquid volume flow rates and 10 different gas flow rates in case without liquid flow. Fig. 4

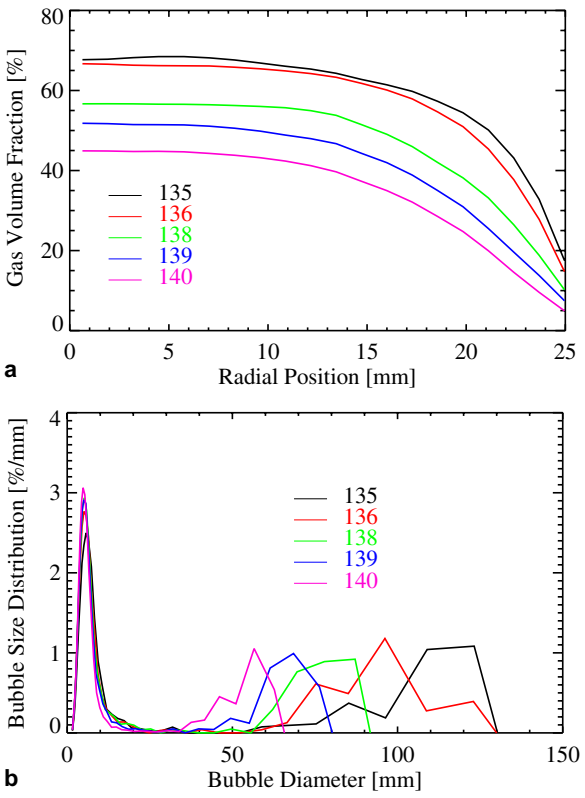

Fig. 12. Radial gas volume fraction profiles and bubble size distributions for slug flow. (Numbers for the points in the measuring matrix see Fig. 4.)

shows the test matrix and indicates the groups of capillaries used for the gas injection. The given superficial velocities always refer the values at normal conditions. The measurements were conducted for up to 10 different distances from the gas injection ($L/D = 0.6$, 1.6, 2.5, 4.5, 8.4, 16.2, 29.9, 39.6, 49.4, 59.2). The measuring time was always 10 s, giving a matrix of raw data with the dimension of $24 \times 24 \times 25.000$ for each sensor. As mentioned above, two sensors were always arranged close together to enable the measurement of correlating the signals used for the determination of the gas velocity. For 10 combinations of gas and liquid flow rates the measurements were repeated eight times to increase the effective measurement time to 80 s.

4. Results

4.1. Observed flow structures

The structure of vertical pipe flow can be characterized by so called flow patterns. Stationary flow pattern maps predict such structures in most cases with dependence on the gas and liquid superficial velocities only (see e.g. Taitel et al., 1980). They are only valid for fully developed flows. The definition of the flow patterns depends on the subjective judgement of the observer

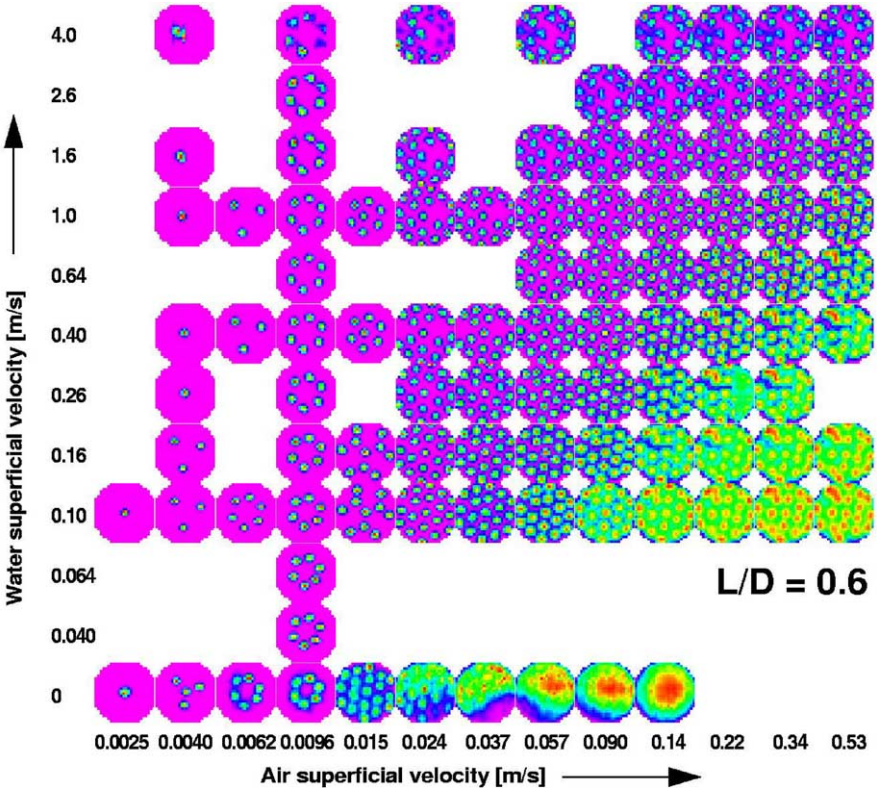

Fig. 13. Time averaged gas volume fraction within the pipe cross-section for $L/D = 0.6$.

especially in transition regions. The new measuring techniques allowed a more objective definition of the flow patterns. The test series discussed in this paper aimed for bubbly and slug flow. Churn turbulent and annular flow were not observed in case of the combinations of volume flow rates shown in Fig. 4. The possibility to measure bubble size distributions allows the definition of the transition between bubbly and slug flow with dependencies on the largest bubbles observed. If bubbles with an equivalent diameter (see Eq. (1)) larger than the pipe diameter occur, the flow pattern is defined as slug flow (Krüssenberg et al., 1999). Otherwise it is defined as bubbly flow. In case of slug flow two peaks always characterize the bubble size distribution—one for the large slug bubbles and one for small bubbles.

Bubbly flow can be divided again into characteristic sub-patterns. A bimodal bubble size distribution was not only observed in case of slug flow, but also if bubbles larger than about 20 mm in equivalent bubble diameter occur (cap bubbles). This sub pattern will subsequently be referred to as "bimodal". The radial gas volume fraction profile has a central peak in this case. A further classification of the sub flow pattern is given by this profile. Here the central peak, wall peak and a transition region can be distinguished by the occurrence of the peak's location or by a flat profile in the radial gas volume fraction. Finally at high liquid volume flow rates (4 m/s) finely dispersed bubbly flow is observed that is characterized by the occurrence of small bubbles and an intermediate peak of the radial gas volume fraction profile. Table 1 summarizes all these flow

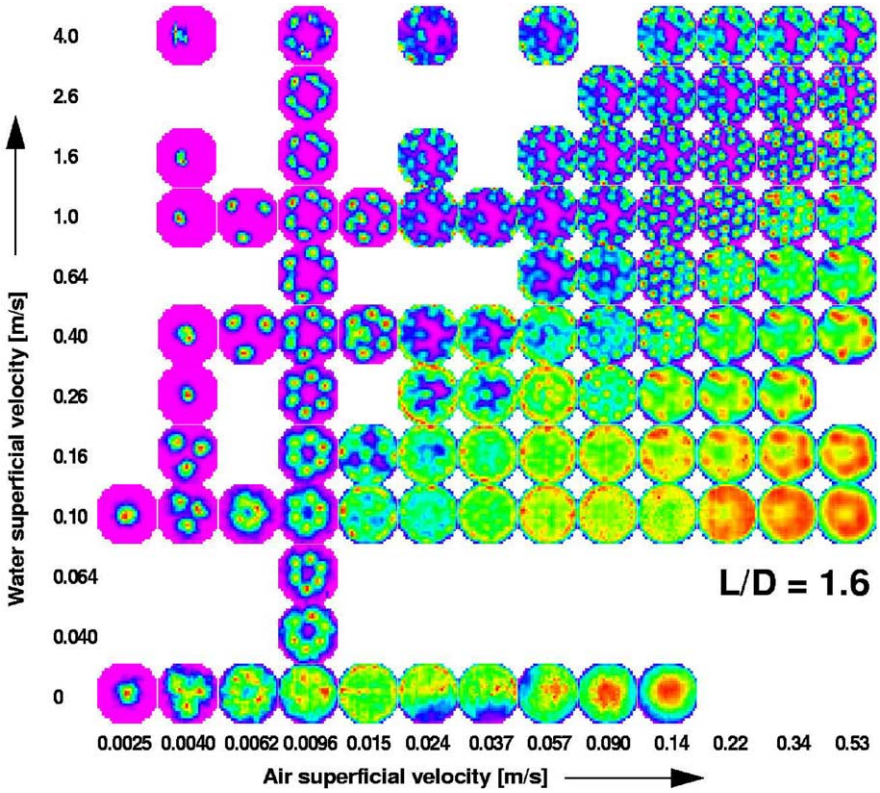

Fig. 14. Time averaged gas volume fraction within the pipe cross-section for $L/D = 1.6$.

patterns and gives the parameter for the examples shown in Fig. 5. In this figure virtual side projections of the measured gas fraction matrix $\varepsilon_{i,j,k}$ are shown (left columns). These images were obtained by a ray-tracing algorithm simulating the virtual propagation of light in a three-dimensional gas fraction distribution. For simplicity it was assumed that a parallel beam of white light arrives from the left side. The red, green and blue components of the light are attenuated by absorption and scattered towards the observer according to virtual absorption and scattering coefficients. The method supplies instructive 3D imaging. More details on the algorithm have been published by Prasser et al. (2005b). The columns on the right hand side show a cut over the pipe cross-section. Examples for the radial gas volume fraction profiles and bubble size distributions that are characteristic of for the single flow patterns are given in the next section.

4.2. Flow at the upper end of the pipe

The flow patterns observed at the upper end of the pipe (3.03 m; $L/D \sim 60$) are shown in Fig. 6. The experimental points were classified according to the flow patterns definitions given in the previous section. Finely dispersed bubbly flow occurs only at the highest superficial water velocities. This agrees with the well known flow map from Taitel et al. (1980).

Radial gas volume fraction profiles are shown in Fig. 7. They are characterized by a maximum at about $R/2$, where R is radius of the pipe. The bubble sizes are below 6 mm in terms of the equivalent bubble diameter.

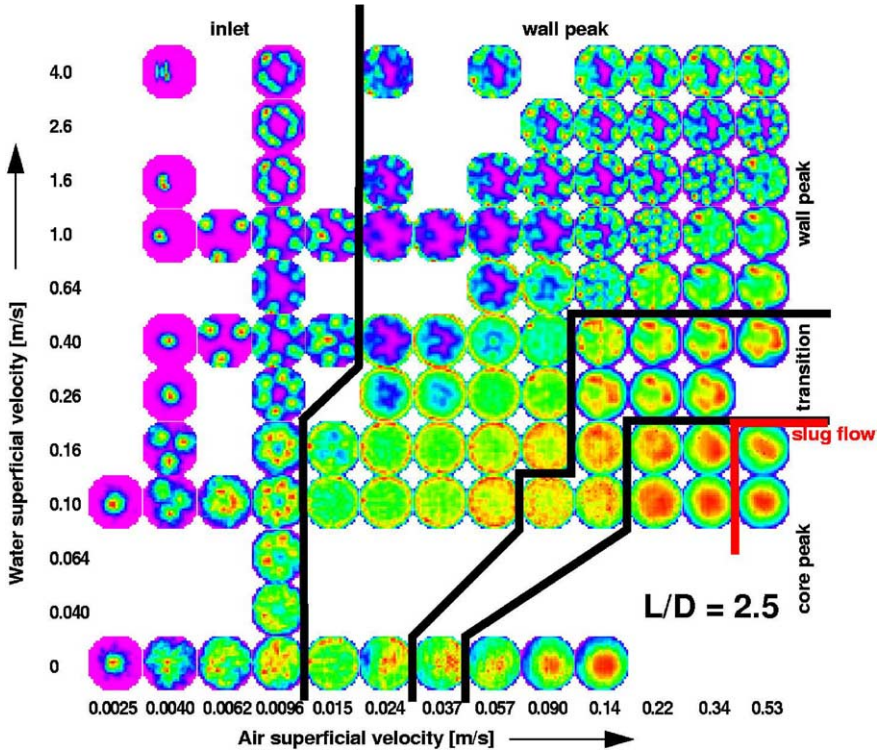

Fig. 15. Time averaged gas volume fraction within the pipe cross-section for $L/D = 2.5$.

Borderlines between the different patterns of bubbly flow and slug flow closely follow lines of constant gas volume fraction with trends from the lower left to the upper right of the measuring matrix (Fig. 6). The boundaries of flow patterns that are caused by the action of wall shear differ from lines of constant gas fraction, like those of finely dispersed flow and the wall peak region. The latter is characterized by different profiles forms with more or less pronounced wall peaks as shown in Fig. 8. Again the bubble sizes are less than 6 mm of equivalent bubble diameter.

A transition to central peak is observed with increasing gas fraction (Fig. 9). This is caused by bubble coalescence, which results in bubble sizes above the critical 6 mm to form, for which the lift force changes sign (Tomiyama, 1998). The onset of coalescence is observed in the bubble size distribution by the appearance of a double peak. The peak at the lower bubble diameter represents the primary bubbles, the second peak belongs to bubbles generated by coalescence of pairs of primary bubbles, the diameter of which is increased approximately by a factor of the cube root of two. The larger bubbles (second peak) can preferred be found in the central region of the pipe, while the smaller bubbles stay closer to the wall (see Fig. 9c). Thus in the transition region radial gas fraction profiles show two peaks as well.

The centre peak region with a mono-modal bubble size distribution (Fig. 10) is followed by a region with a bimodal bubble size distribution (Fig. 11). At high gas volume fractions, slug flow (Fig. 12) is observed. Primarily the transitions do not depend on the total gas fraction, but on the range of bubble sizes observed. This will be discussed more in detail in Section 4.4.

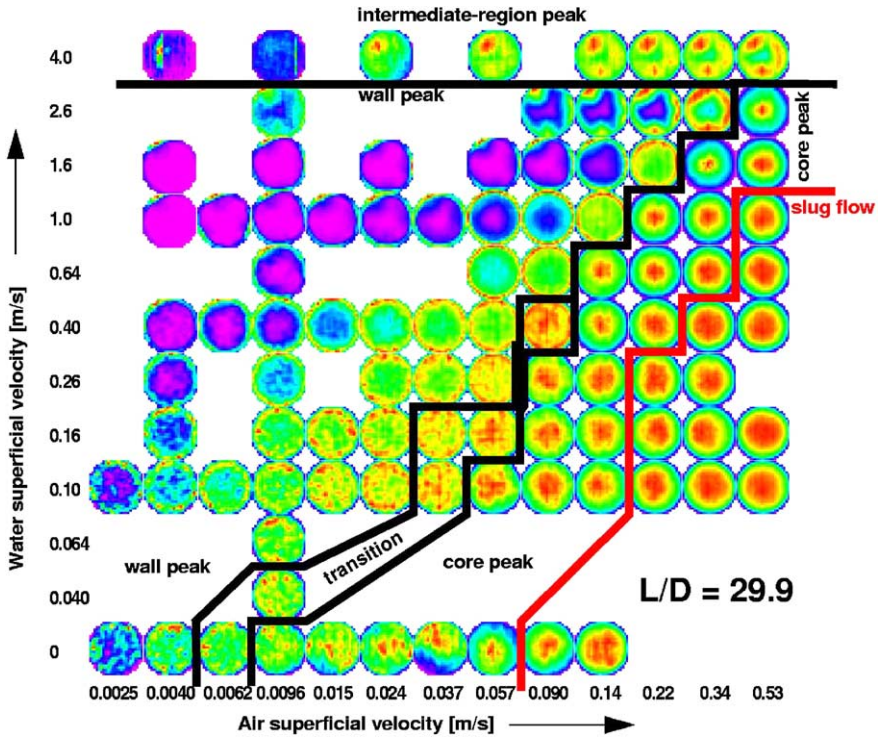

Fig. 16. Time averaged gas volume fraction within the pipe cross-section for $L/D = 29.9$.

4.3. Development of the flow along the pipe

4.3.1. Development of the flow patterns

Figs. 13–17 show the two-dimensional time averaged gas volume fraction distributions over the pipe cross-section for 5 of the 10 different distances between the gas injection device and wire-mesh sensor. The figures show gas volume fractions that are normalized to the maximum of the given test point, since the differences in the total void fraction vary significantly within the matrix. Close to the injection device (Figs. 13 and 14) the distribution still maintains the geometrical pattern of the injection capillary arrangement. Fig. 13 clearly indicates the active groups of capillaries. At $L/D = 1.6$ (Fig. 14) a redistribution of the bubbles can already be observed for most of the cases, but the flow situation is still transient and no clear assignment to flow patterns is possible for this distance. Nevertheless, this data is valuable for the validation of CFD codes, since the models for the forces acting on the bubbles have to reflect the fast redistribution of the bubbles.

Starting from $L/D = 2.5$ a characteristic flow structure can be assigned to an increasing number of combinations of superficial velocity. For very high total gas volume fractions (30–40%) slug flow is observed starting at $L/D = 2.5$. For most points the small bubbles first move towards the wall and form a wall peak. The borderlines for the transition from wall to core peak and from bubbly to slug flow are shifted from the lower right to the upper left with an increasing distance between gas injection and wire-mesh sensor. Some matrix points even pass through all the flow

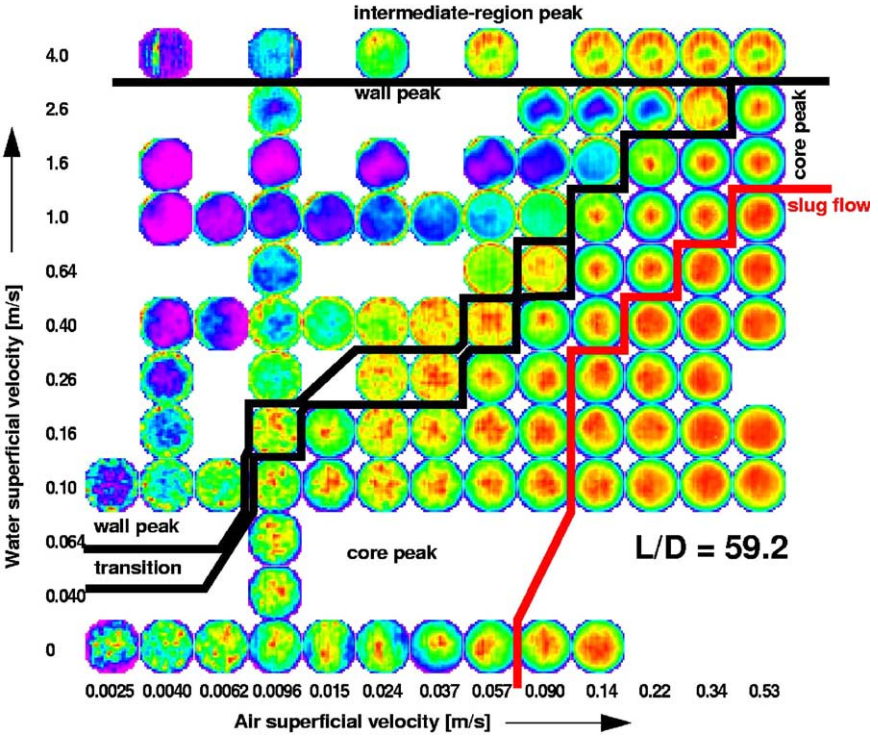

Fig. 17. Time averaged gas volume fraction within the pipe cross-section for $L/D = 59.2$.

regimes from wall peak via transition to core peak and finally to arrive in the slug flow region, like point 140 ($J_L = 1$ m/s, $J_G = 0.53$ m/s). The intermediate peak in the radial gas fraction profile is characteristically found at high liquid superficial velocities and develops from $L/D = 30$ for finely dispersed flow.

From this data, a transient borderline for the transition between bubbly and slug flow can be derived. By Taitel et al. (1980) the border is given for a fully developed flow as

$$J_L = 3.0 J_G - 1.15 \left(\frac{g(\rho_L - \rho_G)\sigma}{\rho_L^2} \right)^{1/4} \tag{4}$$

where J_L and J_G are the liquid and gas superficial velocities, g is the acceleration of gravity, ρ the density and σ the surface tension. These curve agrees very well with the measurements for $L/D = 60$. The shift of the borderline for smaller L/D can be reproduced for all the measured distances by a modification of the first term of the r.h.s in this equation:

$$J_L = 3.0 \sqrt{\frac{L/D - 1}{60}} J_G - 1.15 \left(\frac{g(\rho_L - \rho_G)\sigma}{\rho_L^2} \right)^{1/4}. \tag{5}$$

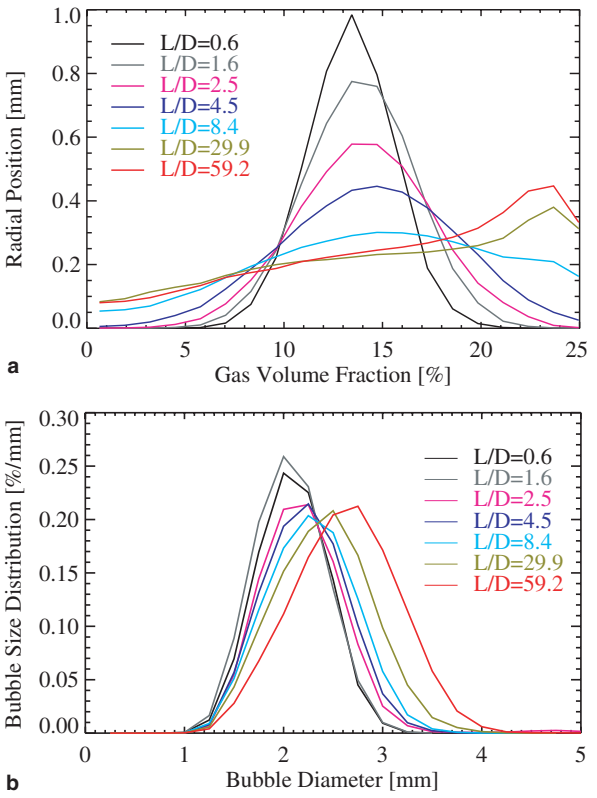

Fig. 18. Development of the radial gas volume fraction profile and the bubble size distribution along the height of the pipe in case of stable bubbly flow at the upper end of the pipe. (Point 043 of the measuring matrix, Fig. 4.)

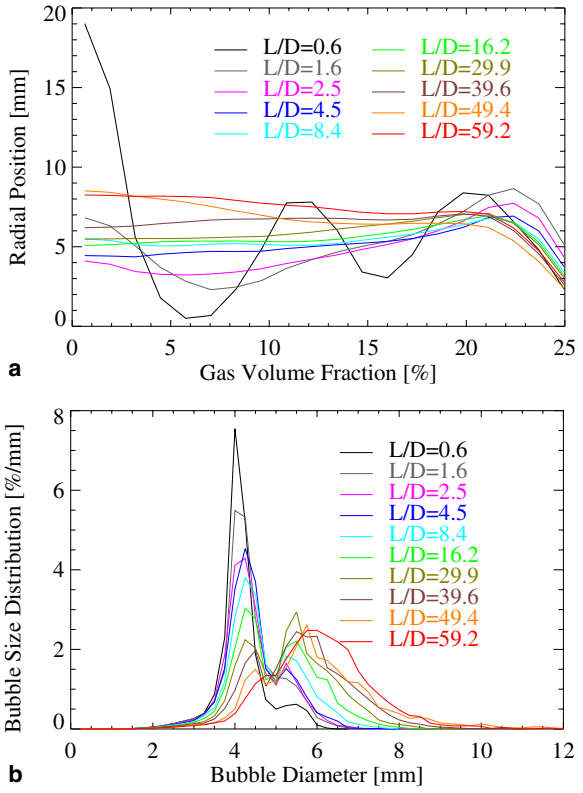

Fig. 19. Development of the radial gas volume fraction profile and the bubble size distribution along the height of the pipe in case of developing bubbly flow at the upper end of the pipe. (Point 071 of the measuring matrix, Fig. 4.)

4.3.2. Development of bubble size distributions and radial gas volume fraction profiles

Typical examples for the development of the radial gas fraction dispersion and the bubble size distribution are shown in Figs. 18–20. Fig. 18 shows an example for stable bubble flow. The small shift of the bubble size distribution is not caused by coalescence, but related to the decreasing pressure. The slight increase in the bubble size is partly due to the change in hydrostatic pressure with increasing height. A stable wall peak of the gas fraction is observed. In the case shown in Fig. 19, a stable bubble size distribution is not yet established even at $L/D = 60$. The bubble sizes still increase because of coalescence. Again, the double peak is caused by the coalescence of pairs of primary bubbles. The shape of the initial radial gas fraction dispersion is still dependent on the distribution of the capillaries for the gas injection.

Examining bubble motion along the flow path, first a wall peak is established that becomes a core peak soon afterwards. It is assumed that the flow pattern would then change to slug flow, if the pipe has a sufficient length. Such a transition to slug flow is demonstrated in Fig. 20. In this case slugging first appears at $L/D = 29.9$. The transition is forced by a high gas fraction in the core region of the pipe ($L/D = 8.4$–16.2). This is caused by the inverted lift force, which pushes the large bubbles ($d > 5.5$ mm in case of air/water flow at ambient conditions) to the centre of the

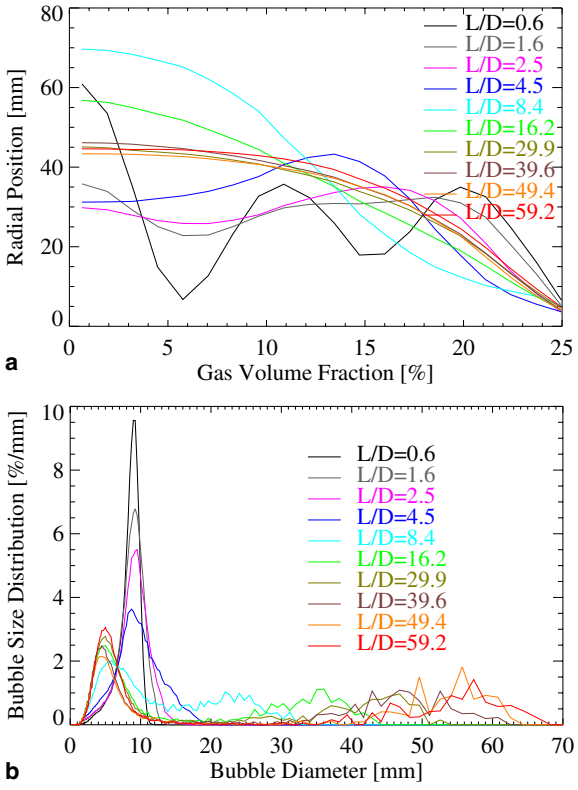

Fig. 20. Development of the radial gas volume fraction profile and the bubble size distribution along the height of the pipe in case of slug flow at the upper end of the pipe. (Point 140 of the measuring matrix, Fig. 4.)

pipe. Bubbles with an equivalent diameter smaller than the initial diameter are generated by break-up from the large bubbles and slugs.

Again, at the upper end of the pipe the flow cannot be assumed to be fully developed. The radial migration of the bubbles is a relatively fast process and equilibrium of the lateral bubble forces can be assumed to be as a good approximation for the upper end of the pipe. Bubble coalescence and fragmentation on the other hand are not in equilibrium except the points in the upper left corner of the matrix where a stable bubbly flow is observed and for the finely dispersed bubbly flow (i.e. no coalescence or equilibrium between coalescence and break-up occurs). There is even a further development in case of slug flow. For the point 135 ($J_L = 0.102$ m/s, $J_G = 0.534$ m/s), which is the point with the highest total gas volume fraction, slug flow starts at $L/D = 2.5$. Fig. 21 shows the measured gas volume fraction averaged over the cross-section of the pipe as a function of time for the three uppermost height positions. The Taylor bubbles always pass the sensor when the high gas volume fraction is measured. The coalescence of the Taylor bubbles causes their number to decrease with height. Over the 10 s time period of each measurement at $L/D = 39.6$, 17 Taylor bubbles pass through the sensor, 14 at $L/D = 49.4$ and 11 at $L/D = 59.2$. Therefore, the Taylor bubbles unite on their way up the pipe.

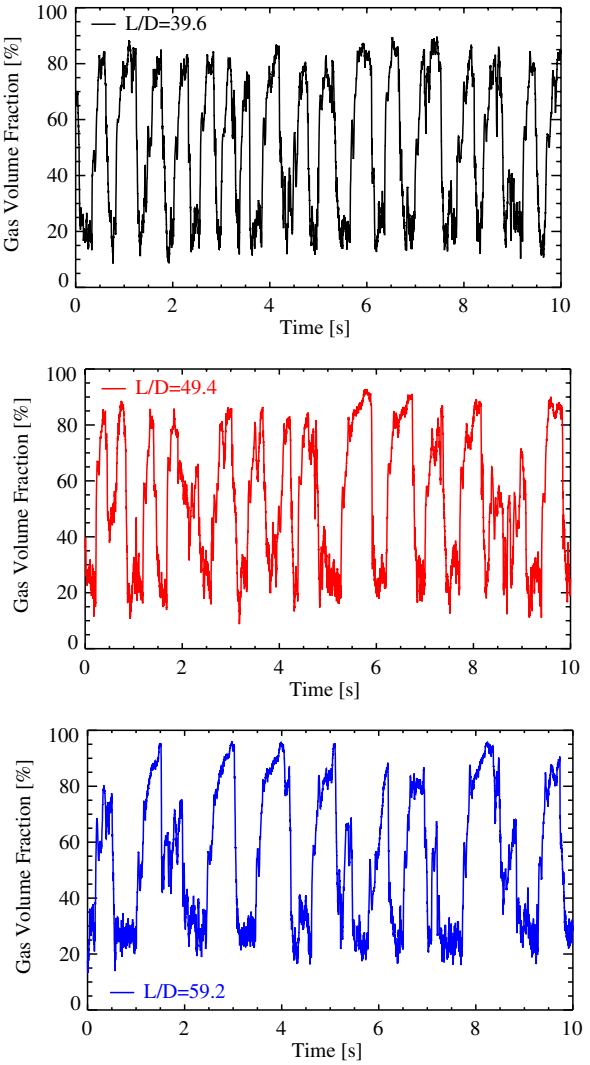

Fig. 21. Gas volume fraction averaged over the pipe cross-section in dependency on the time (point 135 of the measuring matrix, Fig. 4).

4.4. Decomposed volume fraction profiles

Radial volume fraction profiles are decomposed according to the bubble size to give a very detailed insight into the microscopic characteristics of the flow. Such data is produced for bubble classes with a width of 0.25 mm. Radial gas volume fraction profiles for a wider range of bubble sizes are obtained by integrating over more than one of these classes.

Fig. 22 gives an example of the decomposed profiles obtained at the upper end of the pipe. While the total profile has a central peak of the gas volume fraction, decomposed profiles have a more complex behaviour. For the two profiles that represent bubbles with an equivalent diameter less

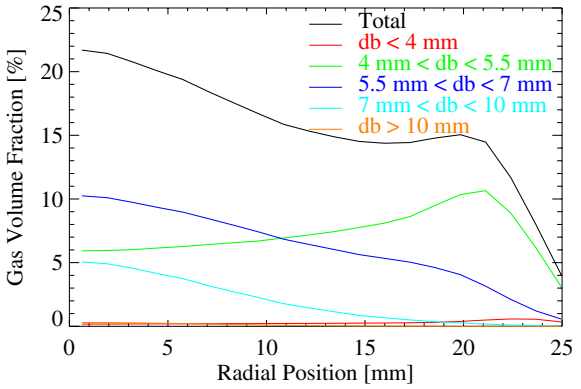

Fig. 22. Profiles of the gas volume fraction decomposed according to the bubble size (point 107 of the measuring matrix, Fig. 4, upper end of the pipe).

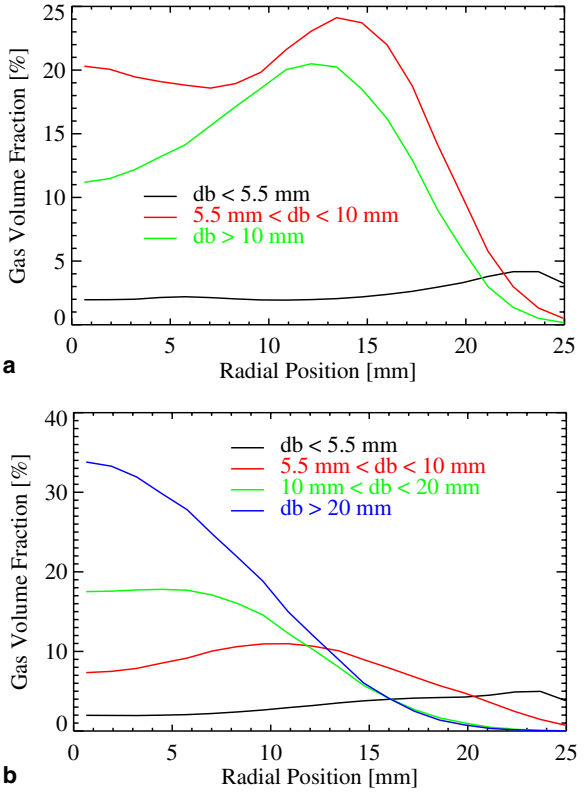

Fig. 23. Profiles of the gas volume fraction decomposed according to the bubble size for $L/D = 4.5$ and $L/D = 8.4$ (point 140 of the measuring matrix, Fig. 4).

than 5.5 mm a clear wall peak is observed. The profiles for larger bubbles form a central peak. This confirms, that the observations made by Tomiyama for single bubbles, are also valid for heavily laden flows with broad bubble size distributions.

This is important for the development of the flow. Injected small bubbles migrate to the wall. There, some larger bubbles are generated by coalescence. Particularly as the coalesced bubbles migrate towards the pipe centre, where further coalescence and lower break-up frequencies (because of the lower shear rates in the central region) create favourable conditions for bubble sizes to grow and to form slugs.

Fig. 23 shows an example of such a migration of large bubbles, which are generated near the pipe wall, towards the pipe centre. The development of the total gas volume fraction profile and the bubble size distribution over the height of the pipe was shown in Fig. 20. There is a very high gas volume fraction in the centre of the pipe at $L/D = 8.4$. Fig. 23 gives the explanation why this larger central peak is formed by bubbles larger than 10 mm (Fig. 23b). Such large bubbles are generated by coalescence on the way from the wall region to the pipe centre (Fig. 23a).

5. Conclusions

An extensive database for air–water bubbly and slug flow in a vertical pipe of 51.2 mm inner diameter was generated. The data include radial gas volume fraction profiles, bubble size distributions and also gas fraction profiles decomposed with regard to each bubble size considered. Since measurements were taken for up to 10 different inlet lengths the transient evolution of the flow along the pipe is reflected by this data. Thus, allowing the classification of a flow pattern according to objective criteria. The measurements clarify the limitations of static flow pattern maps. A correlation for the transition between bubbly and slug flow that was dependant on L/D was obtained.

The experiments confirm the change of the sign of the lift force in relation to the bubble size for the case of a poly-dispersed flow, previously found in experiments on single bubbles by Tomiyama (1998). Small bubbles tend to be found near to the wall region, while larger bubbles tend to concentrate in the core of the pipe.

The data are suitable for the development of closure models for CFD codes. They have already been used for the development and validation of models for the forces acting on the bubbles in the liquid flow field (Lucas and Prasser, 2004; Lucas et al., 2004). Further numerical studies are planned to validate models of bubble coalescence and break-up. At present more measurements are being performed at the new TOPFLOW facility (Schaffrath et al., 2001) for longer pipes up to 8 m and for pipes with a diameter of 194 mm (Prasser et al., 2003, Prasser, 2004).

References

Chang, H., Hills, J.H., Azzopardi, B.J., 1998. A study of the bubble-to-slug transition in vertical gas–liquid flow in columns of different diameter. Int. J. Multiphase flow 24, 431–452.

Ervin, E.A., Tryggvason, G., 1997. The rise of bubbles in a vertical shear flow. J. Fluids Eng. 119, 443–449.

Frank, T., Shi, J.-M., Burns, A.D., 2004. Validation of Eulerian multiphase flow models for nuclear safety applications. In: 3rd International Symposium on Two-Phase Flow Modelling and Experimentation, Pisa, Italy, 22–24 September.

Hibiki, T., Ishii, M., 1999. Experimental study on interfacial area transport in bubbly two-phase flows. Int. J. Heat Mass Transfer 42, 3019–3035.

Krepper, E., Lucas, D., Prasser, H.-M., 2005. On the modelling of bubbly flow in vertical pipes. Nucl. Eng. Design 235, 597–611.

Krüssenberg, A.-K., Prasser, H.-M., Schaffrath, A., 1999. A new criterion for the bubble slug transition in vertical tubes. In: 9th International Topical Meeting on Nuclear Reactor Thermal Hydraulics (NURETH-9), San Francisco, CA, 3–8 October.

Lucas, D., Prasser, H.-M., 2004. Scaling effects in vertical bubbly pipe flow. In: 5th International Conference on Multiphase Flow, ICMF'04, Yokohama, Japan, 30 May–4 June, Paper No. 187.

Lucas, D., Krepper, E., Prasser, H.-M., 2001a. Prediction of radial gas profiles in vertical pipe flow on basis of the bubble size distribution. Int. J. Therm. Sci. 40, 217–225.

Lucas, D., Krepper, E., Prasser, H.-M., 2001b. Development of bubble size distributions in vertical pipe flow by consideration of radial gas fraction profiles. In: 4th International Conference on Multiphase Flow, New Orleans, 27 May–1 June, Conference-CD, Paper 378.

Lucas, D., Krepper, E., Prasser, H.-M., 2003a. Evolution of flow patterns, gas fraction profiles and bubble size distributions in gas–liquid flows in vertical tubes. Trans. Inst. Fluid-Flow Mach. 112, 37–46.

Lucas, D., Krepper, E., Prasser, H.-M., 2003b. Modelling of bubble flow in vertical pipes. In: The 10th International Topical Meeting on Nuclear Reactor Thermal Hydraulics (NURETH-10), Seoul, Korea, paper A00301.

Lucas, D., Shi, J.-M., Krepper, E., Prasser, H.-M., 2004. Models for the forces acting on bubbles in comparison with experimental data for vertical pipe flow. In: 3rd International Symposium on Two-Phase Flow Modelling and Experimentation, Pisa, Italy, 22–24 September.

Ohnuki, A., Akimoto, H., 2000. Experimental study on transition of flow pattern and phase distribution in upward air–water two-phase flow along a large vertical pipe. Int. J. Multiphase flow 26, 376–386.

Prasser, H.-M., 2004. Influence of the gas injection on the void fraction profiles and bubble size distributions of a air–water flow in vertical pipes. In: 5th International Conference on Multiphase Flow, ICMF'04, Yokohama, Japan, 30 May–4 June 2004, Paper No. 366.

Prasser, H.-M., Böttger, A.., Zschau, J., 1998. A new electrode-mesh tomograph for gas–liquid flows. Flow Measure. Instrument. 9, 111–119.

Prasser, H.-M., Krepper, E., Lucas, D., 2000. Fast wire-mesh sensors for gas–liquid flows and decomposition of gas fraction profiles according to bubble size classes. In: Second Japanese–European Two-Phase Flow Group Meeting Tsukuba, Japan, 25–29 September.

Prasser, H.-M., Scholz, D., Zippe, C., 2001. Bubble size measurement using wire-mesh sensors. Flow Measure. Instrument. 12, 299–312.

Prasser, H.-M., Krepper, E., Lucas, D., 2002. Evolution of the two-phase flow in a vertical tube—decomposition of gas fraction profiles according to bubble size classes using wire-mesh sensors. Int. J. Therm. Sci. 41, 17–28.

Prasser, H.-M., Beyer, M., Böttger, A., Carl, H., Lucas, D., Schaffrath, A., Schütz, P., Weiß, F.-P., Zschau, J., 2003. Influence of the pipe diameter on the structure of the gas–liquid interface in a vertical two-phase pipe flow. In: The 10th International Topical Meeting on Nuclear Reactor Thermal Hydraulics (NURETH-10), Seoul, Korea, 5–9 October, Paper A00308.

Prasser, H.-M., Misawa, M., Tiseanu, I., 2005a. Comparison between wire-mesh sensor and ultra-fast X-ray tomograph for an air–water flow in a vertical pipe. Flow Measure. Instrument. 16, 73–83.

Prasser, H.-M., Beyer, M., Böttger, A., Carl, H., Lucas, D., Schaffrath, A., Schütz, P., Weiss, F.-P., Zschau, J., 2005b. Influence of the pipe diameter on the structure of the gas–liquid interface in a vertical two-phase pipe flow. Nucl. Technol. 152, 3–22.

Schaffrath, A., Krüssenberg, A.-K., Weiß, F.-P., Hicken, E.-F., Beyer, M., Carl, H., Prasser, H.-M., Schuster, J., Schütz, P., Tamme, M., 2001. TOPFLOW—a new multipurpose thermal–hydraulic test facility for the investigation of steady state and transient two phase flow phenomena. Kerntechnik 6, 209–213.

Shi, J.-M., Frank, T., Krepper, E., Lucas, D., Rohde, U., Prasser, H.-M., 2004. Implementation and validation of non-drag interfacial forces in CFX-5.6. In: 5th International Conference on Multiphase Flow, ICMF'04, Yokohama, Japan, 30 May–4 June, Paper No. 400.

Sekoguchi, K., Mori, K., 1997. New development of experimental study on interfacial structure in gas–liquid two-phase flow. In: 4th International Conference on Experimental Heat Transfer, Fluid Mechanics and Thermodynamics, Brussels, Belgium, Proceedings, vol. 2, 2–6 June, pp. 1177–1188.

Taitel, Y., Barnea, D., Dukler, A.E., 1980. Modelling flow pattern transitions for steady upward gas–liquid flow in vertical tubes. AIChE J. 26, 345–354.

Tomiyama, A., 1998. Struggle with computational bubble dynamics. In: Third International Conference on Multiphase Flow, ICMF'98, Lyon, France, 8–12 June.

Yoneda, K., Yasuo, A., Okawa, T., Zhou, S.-R., 2000. Flow structure of developing steam-water two-phase flow in a large-diameter pipe. In: Proceedings of ICONE 8, 8th International Conference on Nuclear Engineering, Baltimore, MD, USA, 2–6 April, Paper ICONE-8330.